ADVANCED FUNCTIONAL MATERIALS

Supporting Information

for *Adv. Funct. Mater.*, DOI: 10.1002/adfm.202008609

In Situ Observation of Point-Defect-Induced Unit-Cell-Wise Energy Storage Pathway in Antiferroelectric $PbZrO_3$

Xian-Kui Wei, Chun-Lin Jia, Krystian Roleder, Rafal E. Dunin-Borkowski, and Joachim Mayer*

Supporting Information

In-situ Observation of Point-Defect-Induced Unit-Cell-Wise Energy Storage Pathway in Antiferroelectric $PbZrO_3$

Xian-Kui Wei, Chun-Lin Jia, Krystian Roleder, Rafal E. Dunin-Borkowski, and Joachim Mayer*

*Corresponding author E-mail: x.wei@fz-juelich.de

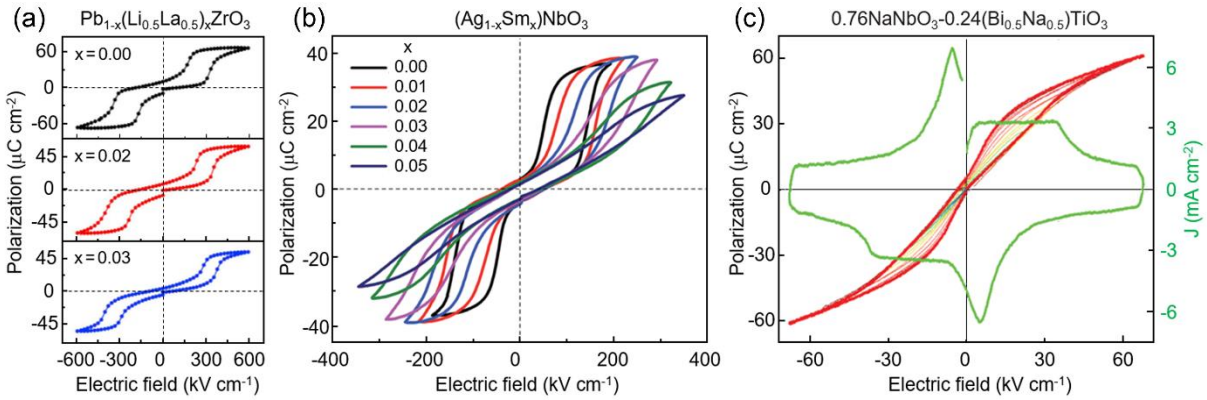

Figure S1. Remnant polarization in typical antiferroelectric materials. a) Polarization-electric field (*P-E*) hysteresis loops of AFE $Pb_{1-x}(Li_{0.5}La_{0.5})_xZrO_3$ with x = 0.00, 0.02 and 0.03.[12] The remnant polarization is in the range of P_r = 3.5 ~ 8.3 μC cm^{-2}. b) The *P-E* hysteresis loops of AFE $(Ag_{1-x}Sm_x)NbO_3$ with x = 0.00, 0.01, 0.02, 0.03, 0.04 and 0.05.[24] The remnant polarization is $P_r \approx$ 2.8 μC cm^{-2}. c) The *P-E* hysteresis loops under different electric fields and current-*E*

curve of $0.76NaNbO_3$-$0.24(Bi_{0.5}Na_{0.5})TiO_3$ relaxor AFE measured at a frequency of 10 Hz.[25] The remnant polarization is $P_r \approx 2.5$ μC cm^{-2}.

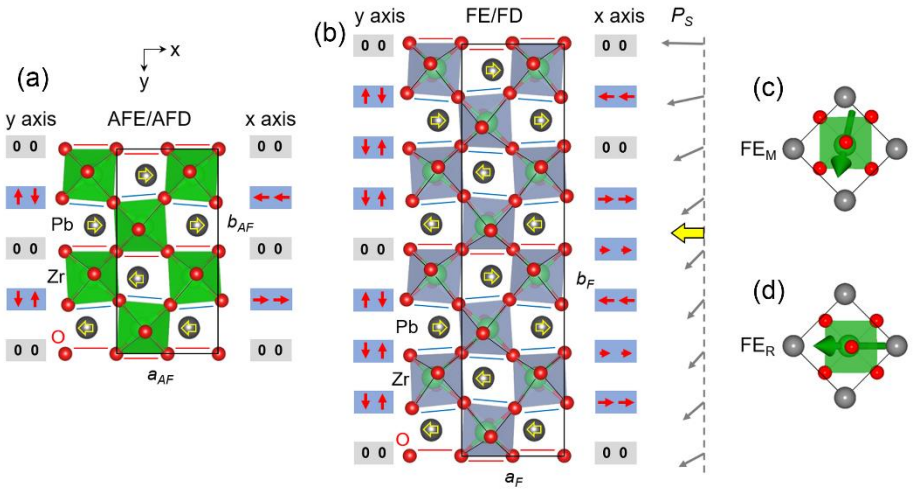

Figure S2. Structure and polarization feature of AFE/AFD, FE/FD, FE_M and FE_R phase of $PbZrO_3$. a,b) Crystal structure of AFE-AFD phase and FE-FD phase of $PbZrO_3$ viewed along the $[001]_O$ direction, respectively. The Pb atoms with antiparallel displacements are denoted by

empty yellow arrows. The red arrows and blue line segments denote the characteristic displacements of oxygen along x and y direction. The zeros "0" and red line segments denote the oxygen atoms locating at the centrosymmetric positions. The x-direction oxygen shift induced unit-cell doubling can be identified from the FE/FD phase shown in (b), which is characteristic of the cycloidal polarization order (grey arrows on the right)[14] with P_S essentially running along the x direction. c,d) Schematic unit cell of the ferroelectric monoclinic (FE_M) and rhombohedral (FE_R) phase, respectively. The P_S in the FE_M phase is flexibly rotatable within the pseudocubic $(110)_p$ crystal plane.

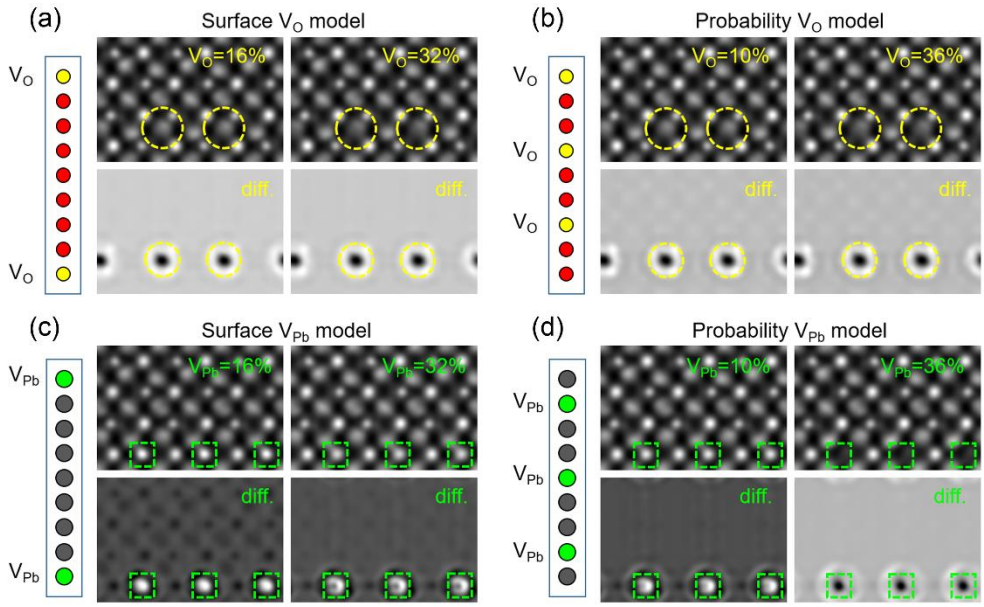

Figure S3. Image simulation based on different vacancy models. a,c) Surface vacancy models with vacancy content of V_O and V_{Pb} at 16% and 32% for the specific column, respectively. b,d) Probability vacancy models with vacancy content of V_O and V_{Pb} at 10% and 36% for the specific column, respectively. With respect to the V_{Pb} = 10% condition, we see the contrast reduction as the V_{Pb} concentration increases to 36% at this specific atomic column. The differences of the vacancy-containing simulated images with the vacancy-free simulated ones are illustrated at the bottom rows. The images are simulated at a specimen thickness of 10.2 nm and a defocus value of 8.5 nm based on the multi-slice method.

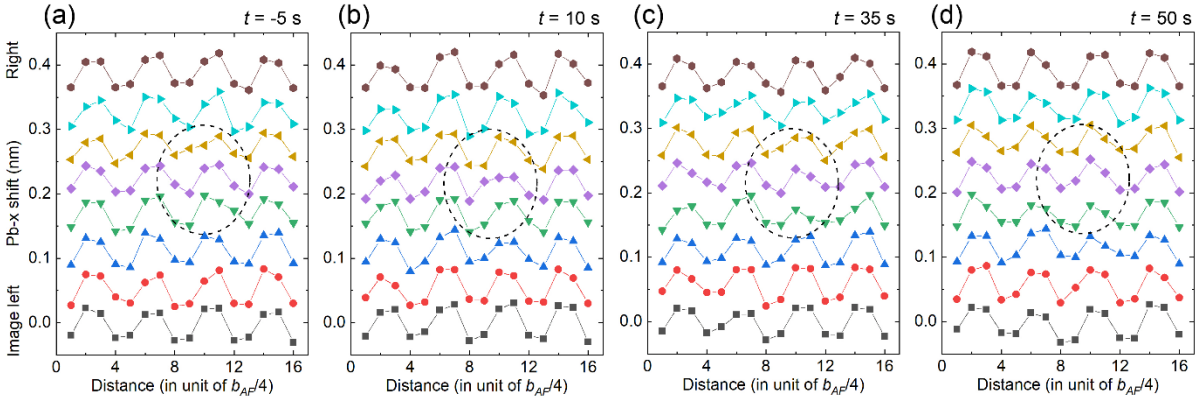

Figure S4. Evolution of antiparallel Pb shifts near the defect core as a function of electron-beam irradiation. a-d) Antiparallel Pb displacements along $[100]_O$ direction plotted as a function of distance along $[010]_O$ direction at irradiation time t = -5, 10, 35 and 50 s, respectively. These

plots correspond to atomic-resolution TEM images shown in Figure 2a,c,e and g, respectively. With respect to the TEM images, the plots shown here are anticlockwise rotated by 90 degree. The dashed black circles denote positions of the defect core, where deviation from the regular Pb shifts can be seen at specific atomic sites.

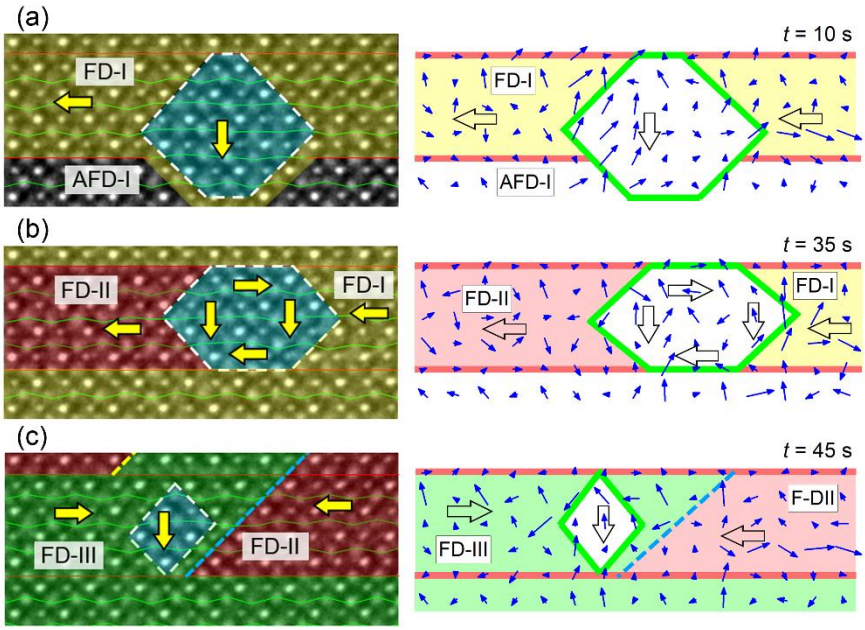

Figure S5. Determination of oxygen polar displacements near the defect core and nearby domains. a-c) The atomic-resolution TEM images near the defect core with recording time at t = 10, 35 and 50 s, annotation of the AFD, FD (yellow, red and green shadows) domain states and orientation of spontaneous polarization derived from mapping of oxygen shifts with respect to centers of the nearest-neighboring Zr columns. The red (thin and thick) and green solid lines denote the shifts of oxygen along y direction. The dashed yellow and blue lines denote the tail-to-tail and head-to-head charged domain walls.

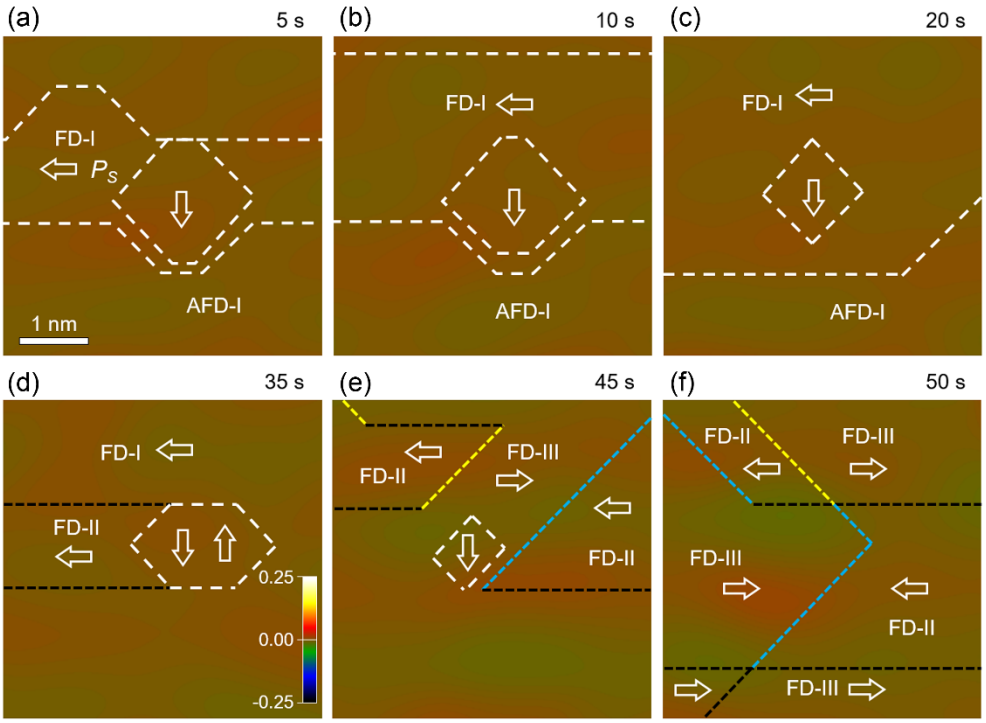

Figure S6. Evolution of lattice strain (e_{yy}) map as a function of electron-beam irradiation time from GPA analysis. a-f) The e_{yy} map (along $[010]_O$ direction) for TEM images recorded at t = 5, 10, 20, 35, 45 and 50 s, respectively. The colorful dashed lines denote the phase boundary (white), defect core (white), transversal (black), tail-to-tail (yellow) and head-to-head (blue) charged domain walls between the ferrodistortive domains, respectively.

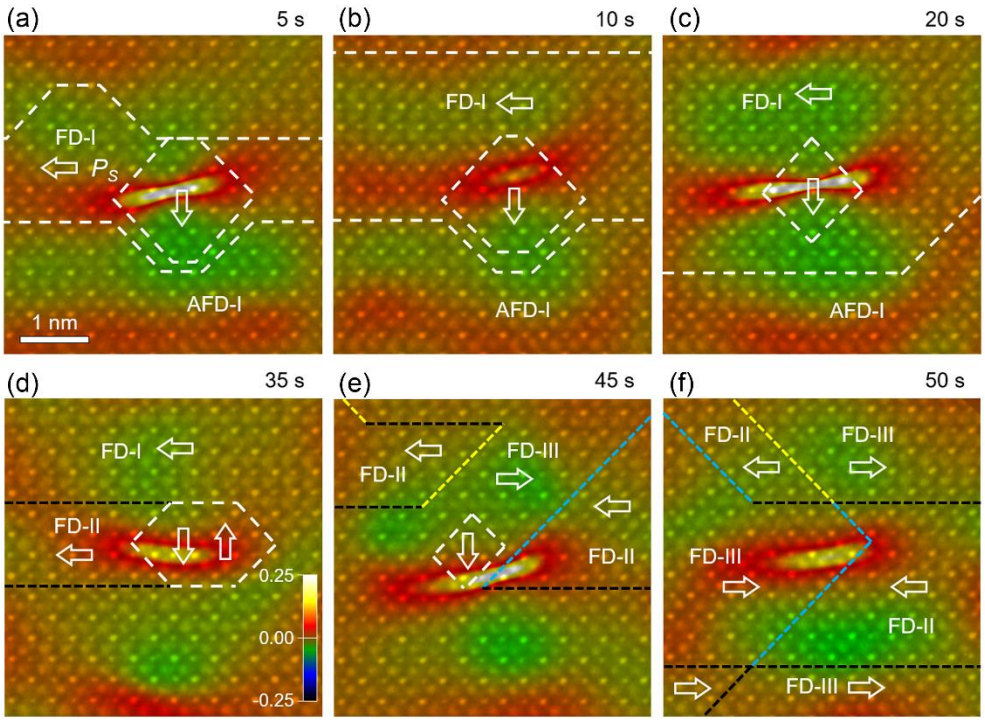

Figure S7. Evolution of lattice rotation (rot_{xy}) map as a function of electron-beam irradiation time from GPA analysis. a-f) The rot_{xy} map for TEM images recorded at t = 5, 10, 20, 35, 45 and 50 s, respectively. The shear strain e_{xy} map shows almost the same behavior as the rot_{xy} map. The colorful dashed lines denote the phase boundary (white), defect core (white), transversal (black), tail-to-tail (yellow) and head-to-head (blue) charged domain walls between the ferrodistortive domains, respectively. Accompanied with presence and growth of the FD domains, dynamic changes of the defect core, e.g., position and length, orientation and local lattice rotation can be clearly seen.

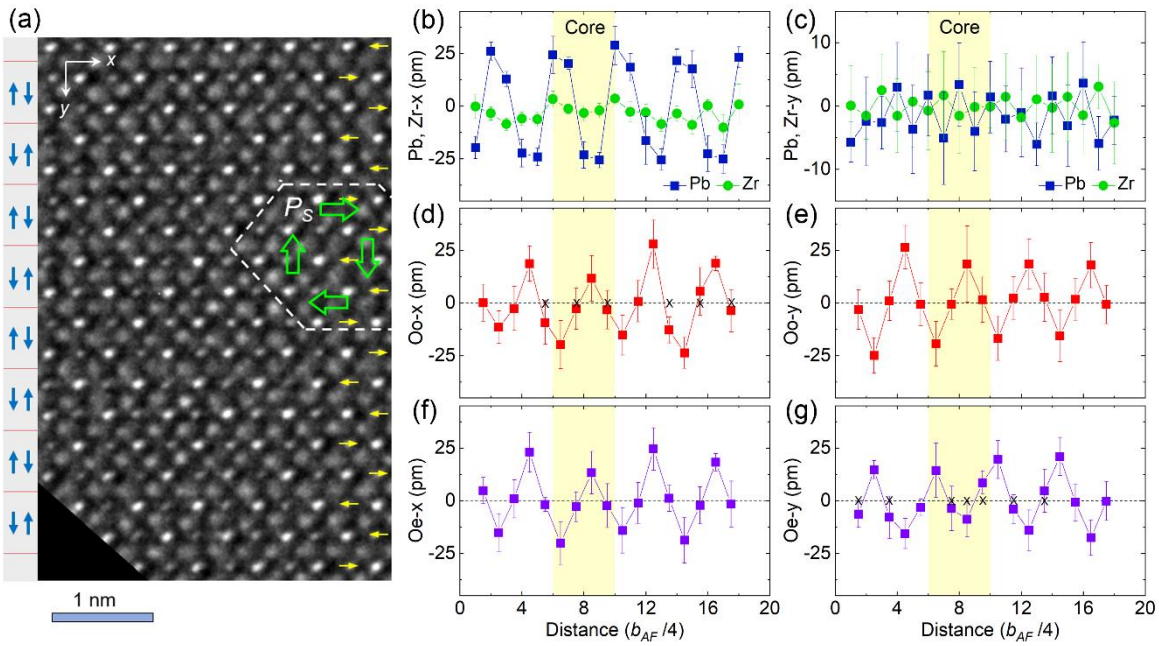

Figure S8. Quantitative analysis on atomic displacements near the defect core for the image recorded at t = -5 s. a) Atomic-resolution TEM image of $PbZrO_3$ recorded along $[001]_O$ direction. The yellow arrows and white dashed line denote the antiparallel Pb shifts and the defect core. The red solid lines and blue arrows denote the oxygen atoms locating at the neutral sites and those undergoing the y-direction shifts, respectively. b,c) Atomic displacements of Pb and Zr atoms along the x//[100] and y//[010] direction, respectively. d-g) Atomic displacements of odd-column (Oo) and even-column oxygen (Oe) atoms along the x and y direction, respectively. The presented data profiles are averaged along the x direction.

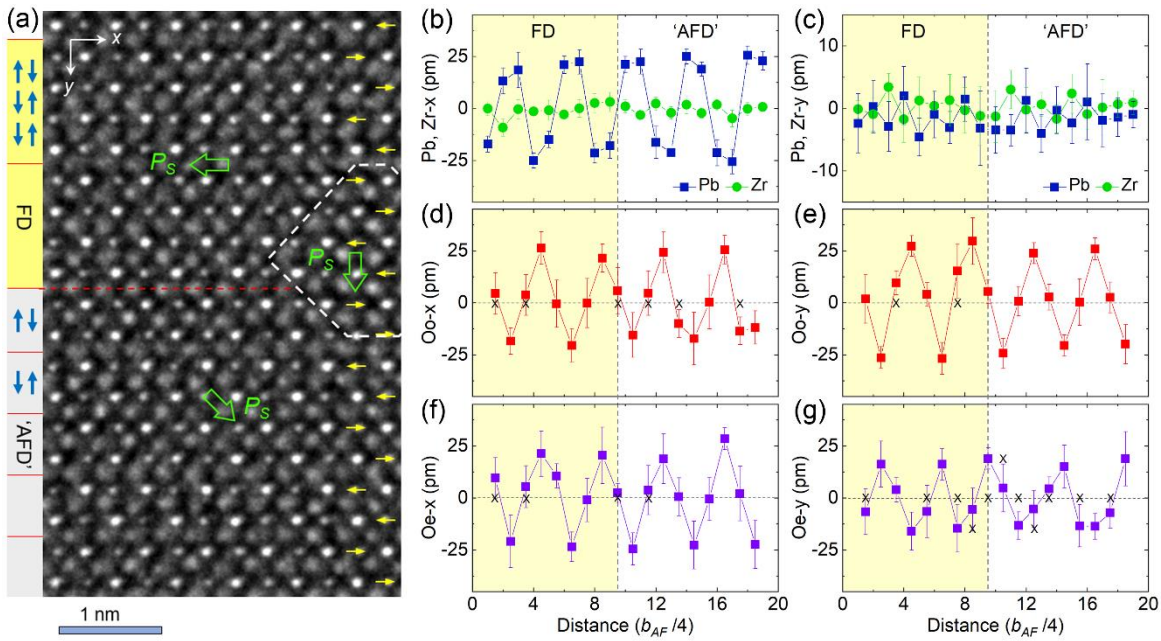

Figure S9. Quantitative analysis on atomic displacements near the defect core for the image recorded at t = 10 s. a) Atomic-resolution TEM image of $PbZrO_3$ recorded along $[001]_O$ direction. The yellow arrows and white dashed line denote the antiparallel Pb shifts and the defect core. The red solid and dashed lines denote the oxygen atoms locating at the neutral sites and the AFD/FD phase boundary, respectively. b,c) Atomic displacements of Pb and Zr atoms along the x//$[100]_O$ and y//$[010]_O$ direction, respectively. d-g) Atomic displacements of Oo and Oe atoms along the x and y direction, respectively. The presented data profiles are averaged along the x direction.

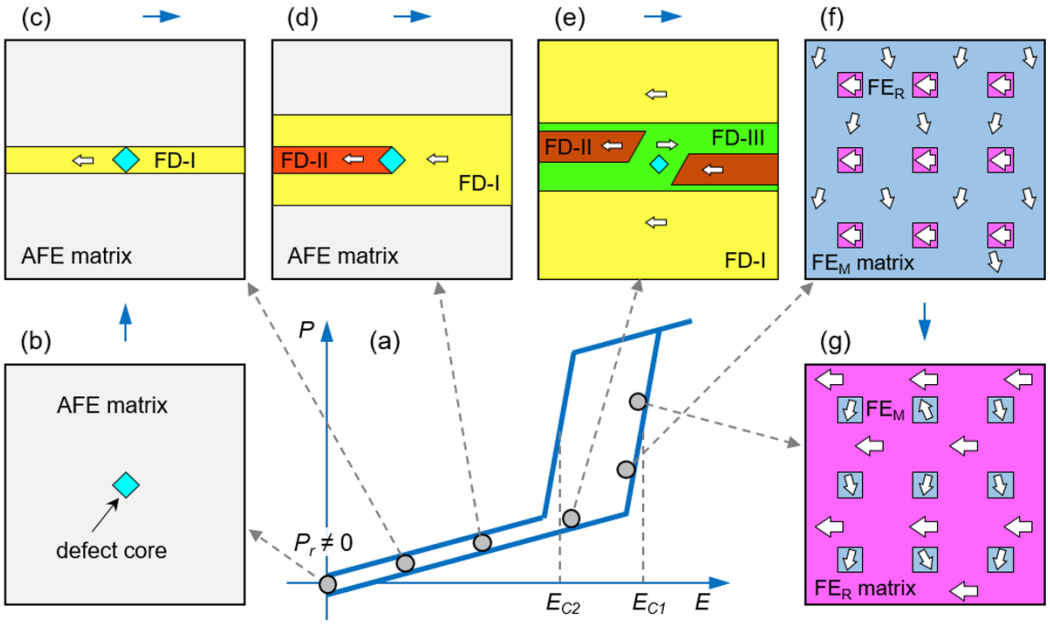

Figure S10. Illustration of energy storage process in $PbZrO_3$ according to experimental observations. a) Schematic hysteresis loop. b-e) Defect core induced AFD-to-FD state transition, growth of FD-I state, generation of FD-II and FD-III states with formation of charged domain walls, respectively. f) FE_M matrix with embedding of FE_R nanoislands. g) FE_R matrix with embedding of FE_M nanoislands. The size of black-stroked white arrows denotes magnitude of the polarization in different FE phases.

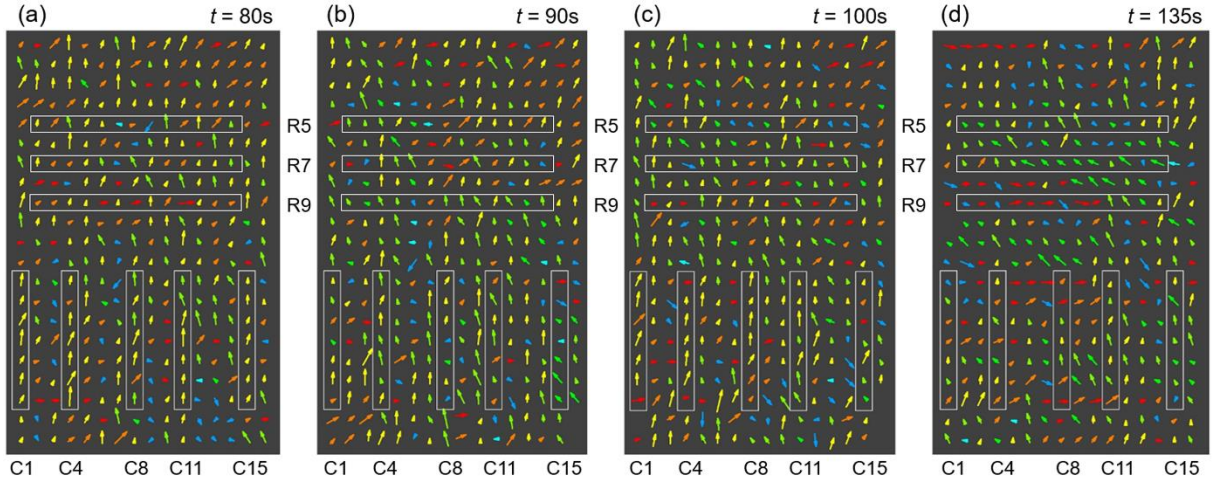

Figure S11. Unit-cell-wise FE_M-to-FE_R transition. a-d) The evolution of oxygen displacements (color arrows) against centers of the nearest-neighboring Zr columns in ordinary FE $PbZrO_3$. To facilitate identifying the unit-cell-wise FE_M-to-FE_R transition, certain atomic columns (C1, C4, C8, C11, C15) and rows (R5, R7, R9) are delineated to track changes of oxygen displacements during the energy-storage process. One can see the unit-cell-wise FE_M-to-FE_R transition, but very regular domain structure change can hardly be identified.

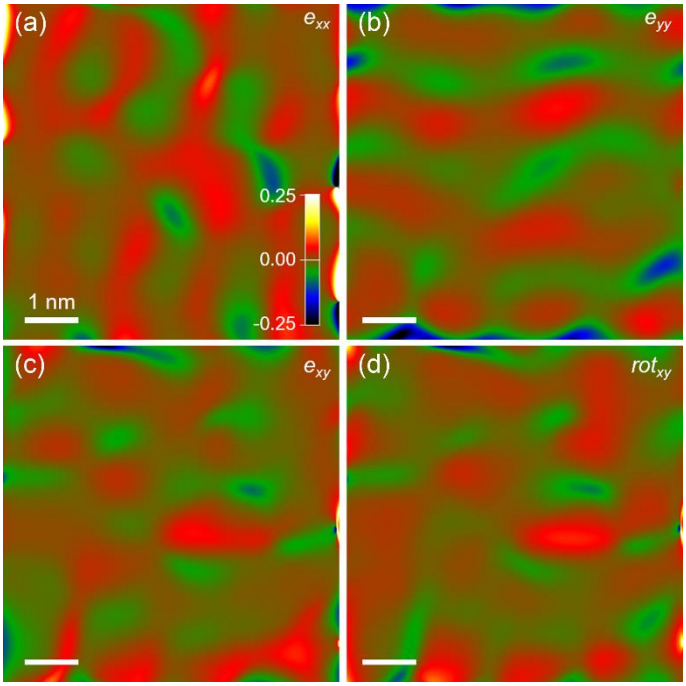

Figure S12. GPA analysis for the FE_M phase recorded at t = 80 s. a-d) The e_{xx}, e_{yy}, e_{xy} and lattice rotation rot_{xy} maps. The x and y directions are selected along $[100]_O$ and $[010]_O$ direction, respectively.

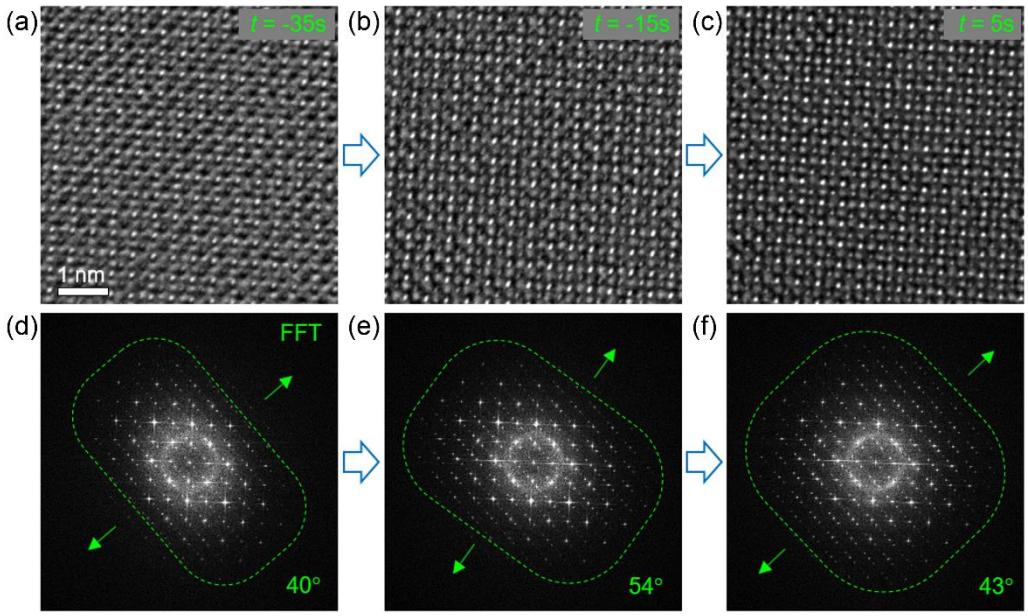

Figure S13. Direct evidence of charging effect of $PbZrO_3$ during irradiation induced energy storage. a-c) Atomic resolution TEM images recorded along the $[001]_O$ direction at t = -35, -15 and 5 s, respectively. d-f) Corresponding fast Fourier transform (FFT) images of (a-c), respectively. The electron beam charging effect leads to cutting of the diffractogram along certain direction. The angles denote the short-axis direction of the green dashed squares, delineating contour of the intensity distribution of diffractogram, away from the horizontal axis.